

# Inhibition of splitting of the chiral and deconfinement transition due to rotation in QCD: the phase diagram of linear sigma model coupled to Polyakov loop

Pracheta Singha,<sup>1</sup> Victor E. Ambrus,<sup>1</sup> and Maxim N. Chernodub<sup>2,1</sup>

<sup>1</sup>*Department of Physics, West University of Timișoara,  
Bd. Vasile Pârvan 4, Timișoara 300223, Romania*

<sup>2</sup>*Institut Denis Poisson UMR 7013, Université de Tours, 37200 France*  
(Dated: July 11, 2024)

We discuss the effect of rigid rotation on critical temperatures of deconfinement and chiral transitions in the linear sigma model coupled to quarks and the Polyakov loop. We point out the essential role of the causality condition, which requires that any point of the system should rotate slower than the velocity of light. We show that imposing this physical requirement leads to inhibition of the splitting between the chiral and confining transitions, which becomes negligibly small ( $\Delta T \sim 1$  MeV or less) for experimentally relevant, slow angular velocities  $\Omega \sim 10$  MeV of a (5–10) fm-sized systems. Moreover, the boundedness of the system has a much bigger effect on temperature splitting than the rotation itself: the splitting reaches 10 MeV in a small, one-fermi-sized non-rotating system. The temperature splitting may, however, become enhanced in an academic limit of ultra-relativistic regimes when the boundary of the system rotates at near-to-light velocities.

## I. INTRODUCTION

The experimental observation of highly vortical quark-gluon plasmas created in non-central heavy-ion collisions has sparked significant theoretical interest in elucidating the properties of this unprecedentedly vortical fluid [1, 2]. The vortical effects of the plasma have been examined through hydrodynamic and transport-based models [3, 4], as well as lattice first-principle approaches rooted in numerical Monte Carlo techniques [5–12].

The strong, non-perturbative nature of quark-gluon plasma precludes the reliable theoretical exploration of its dynamics using conventional, perturbative analytical methods. This constraint necessitates reliance on effective theoretical models that describe the infrared properties of QCD. On the other hand, numerical techniques provide us with information on the behavior of thermodynamic characteristics, such as critical temperature, often without pointing out a physical mechanism that lies behind the numerical data [6–8, 11] (see, however, the conjecture of the negative Barnett effect put forward in Ref. [13]). Although numerical methods often do not directly elucidate the mechanisms underlying non-perturbative effects, the data they generate provide us with invaluable information for constraining effective theoretical models and thereby enhancing our understanding of the underlying physical phenomena. In our paper, we will use one of such models, which is the linear sigma model with quarks [14] improved with a coupling to the Polyakov line (PLSM<sub>q</sub>) [15–19].

The lattice simulations have revealed that vorticity influences the thermodynamic properties and phase structure of quark-gluon plasma in a somewhat unexpected way, as the critical temperature of the deconfining phase transition appears to be a rising function of the angular velocity both for pure gauge theory [6, 7] and for QCD [8, 11]. On the contrary, most theoretical models, including field theoretical approaches and holographic

techniques, predict that the critical temperature should be a diminishing function of the angular velocity [20–28]. This property is readily understood at the level of quarks: the coupling of the intrinsic angular momentum of the constituents of the system to the angular velocity of its global rotation should break the chiral condensate, thus leaving less condensate to be evaporated by the thermal fluctuations. The breaking of the condensate by rotation is a quark analog of the Barnett effect, which tends to polarize spins and orbital momenta in the direction of the angular velocity [29].

The situation on the theoretical side can be improved by phenomenologically tuning the parameters of the system in such a way that the parameters of the original model become dependent on the angular velocity itself [30]. However, similarly to the first-principle numerical approaches, the fine-tuned effective infrared models offer somewhat limited help in elucidating the physical mechanism that lies behind this fine-tuning. On the other hand, the inclusion of couplings that depend on the external parameters (temperature, rotation) aligns well with the logic of the Polyakov-loop improved models in which the Lagrangian that incorporates the dynamics of the loop contains already temperature-dependent couplings [31–33]. In our paper, we consider the traditional sigma model in which the model parameters and couplings do not depend on the external parameters.

The subject of our paper is devoted to the suggestion that the rotation can split the deconfinement and chiral transitions of QCD put forward in Ref. [34]. This hypothesis sounds very reasonable since the global rotation can affect gluons and quarks in different ways, thus forcing the transition to split into the transitions associated, separately, with gluons (the deconfinement transition) and quarks (the chiral transition). On the other hand, Ref. [34] did not consider the boundary effect of the system. The absence of a transverse boundary incurs, in a rigidly rotating case, superluminal velocities of rotating matter that may lead to the appearance of

unphysical artifacts in calculations [35]. One could argue, however, that if the superluminal effect appears at a large enough distance from the center or rotation—as it happens for a slowly rotating system—then the breaking of the causality is not a physically relevant property due to the existence of the finite correlation length in the system. Therefore, the effect of the boundaries on the splitting of the transitions needs to be clarified.

Unfortunately, the PLSM<sub>q</sub> cannot describe the chiral (or chiral and deconfinement) phase transitions even qualitatively. However, this model, similarly to the one considered in Ref. [34], serves as a very successful effective model for characterizing the infrared phenomenology of the non-rotating quark-gluon matter. In this paper, we use it to probe the effects associated with the spatial boundedness of the system in the presence of rotation, and confront them with the results in the unbounded case [34]. Moreover, we expect, given our results below, that the modification of the effective infrared model by introducing environment-dependent couplings will not modify the qualitative conclusions of our paper.

The structure of the paper is as follows. In Section II, we describe the formulation of the PLSM<sub>q</sub> model in a non-rotating system. Section III is devoted to the description of the rigidly rotating environment. To respect the causality, the rigidly rotating system requires the introduction of the boundaries in the transverse plane, which is perpendicular to the angular velocity vector. The cylindrical boundary quantizes the transverse radial modes, leading to a complication of the energy spectrum and requiring extensive numerical computations. In the same section, we show explicitly how quantization emerges in the case of spectral boundary conditions. Section IV investigates the phase diagram, the nature of the phase transitions, and the splitting in chiral and deconfining transitions. The effects of the finite radius of the cylinder, the chemical potential, and, finally, the rotation are studied in detail. The last section is devoted to our conclusions.

## II. THE MODEL

### A. Lagrangian

The Polyakov-loop enhanced linear sigma model coupled to quarks (PLSM<sub>q</sub>) has three types of variables: the quark doublet field  $\psi(x)$ , the  $O(4)$  chiral fields  $\phi = (\sigma, \vec{\pi})$  with the pion isotriplet  $\vec{\pi} = (\pi^+, \pi^-, \pi^0)$ , and the Polyakov loop variable  $L(x)$ . They enter the Lagrangian of the model via the following three terms that are associated with the mentioned variables:

$$\mathcal{L} = \mathcal{L}_\phi(\sigma, \vec{\pi}) + \mathcal{L}_L(L) + \mathcal{L}_q(\psi, \phi, L). \quad (1)$$

In this section, we will briefly describe the properties of the model in the unbounded case.

### 1. Chiral sector

The chiral field  $\phi = (\sigma, \vec{\pi})$  encodes, as it follows from its name, the chiral features of the model, with  $\sigma$  playing the role of an approximate order parameter of the chiral transition. The field  $\sigma$  tends to zero in the large-temperature, chirally restored phase and is non-vanishing in the low-temperature, chirally broken phase. In QCD with realistic masses of quarks, the chiral transition between the two phases is a smooth crossover, implying the absence of a well-defined thermodynamic transition at finite temperatures.

The chiral part of the PLSM<sub>q</sub> Lagrangian is given by the first term of Eq. (1):

$$\mathcal{L}_\phi(\sigma, \vec{\pi}) = \frac{1}{2}(\partial_\mu\sigma\partial^\mu\sigma + \partial_\mu\vec{\pi}\partial^\mu\vec{\pi}) - V_\phi(\sigma, \vec{\pi}), \quad (2)$$

where the phenomenological potential of the chiral fields,

$$V_\phi(\sigma, \vec{\pi}) = \frac{\lambda}{4}(\sigma^2 + \vec{\pi}^2 - v^2)^2 - h\sigma, \quad (3)$$

exhibits both spontaneous and explicit breaking of chiral symmetry. The potential gives a non-zero expectation value for the  $\sigma$  field and provides the masses  $m_\sigma$  and  $m_\pi$  to the sigma and the pion mesons, respectively. Writing  $\sigma = \langle\sigma\rangle + \delta\sigma$  and  $\vec{\pi} = \langle\vec{\pi}\rangle + \delta\vec{\pi}$ , these masses can be obtained from the expansion in terms of small fluctuations  $\delta\sigma$  and  $\delta\pi$ :

$$V = V_0 + \frac{1}{2}m_\sigma^2\delta\sigma^2 + \frac{1}{2}m_\pi^2\delta\vec{\pi}^2 + \dots, \quad (4)$$

with  $V_0 = V(\langle\sigma\rangle, 0) = \frac{\lambda}{4}(\langle\sigma\rangle^2 - v^2)^2 - h\langle\sigma\rangle$  and

$$m_\sigma^2 = \lambda(3\langle\sigma\rangle^2 - v^2), \quad m_\pi^2 = \langle\sigma\rangle^2 - v^2, \quad (5)$$

where we imposed  $\langle\vec{\pi}\rangle = 0$  as it follows from the minimum of potential (3).

The analysis of the linear sigma model is usually done in a mean-field approach, in which the “slow” meson sector is considered a classical field. In contrast, quarks are treated as quantum fields that represent “fast” degrees of freedom. The parameters of Lagrangian (2) are chosen to match the low-energy phenomenology [36]. The masses in Eq. (3) serve as the model parameters that coincide with corresponding meson masses in the vacuum, i.e., at zero temperature,  $T = 0$ , and in the absence of rotation,  $\Omega = 0$ . In particular,  $m_\pi \approx 138$  MeV,  $\langle\sigma\rangle = f_\pi \approx 93$  MeV. In the absence of electromagnetic interactions, the masses of charged,  $\pi^\pm$ , and neutral,  $\pi^0$ , mesons do not split.

The explicit symmetry-breaking term is determined by the PCAC relation,  $h = f_\pi m_\pi^2$ . Consequently, in the vacuum state,  $v^2 = f_\pi^2 - m_\pi^2/\lambda$  and  $m_\sigma^2 = 2\lambda f_\pi^2 + m_\pi^2$ . By selecting the mass of the  $\sigma$  meson  $m_\sigma = 600$  MeV, one gets a reasonable value for the quartic interaction coupling,  $\lambda = 20$ . If the explicit symmetry breaking term were absent,  $h = 0$ , then the model (2) would experience

a second-order phase transition [37] from the chirally broken symmetry phase to the chirally restored phase at the critical temperature  $T_c = \sqrt{2}v$ . The explicit symmetry-breaking term removes the exact chiral  $O(4)$  symmetry of this theory and alters the phase transition into a smooth crossover in consistency with the QCD phenomenology. Notice that the pion fluctuations play no major role in the chiral phase transition [38] for the case of the chiral transition (see also a discussion in Ref. [39]). Therefore, below, we focus only on the sigma direction of the chiral sector.

## 2. Confining sector

The confining properties of the system are accounted for by the second term in Eq. (1), which describes the complex-valued Polyakov loop variable,

$$L(x) = \frac{1}{3} \text{Tr} \Phi(x),$$

$$\Phi = \mathcal{P} \exp \left[ i \int_0^{1/T} dx_4 \mathcal{A}_4(\vec{x}, x_4) \right]. \quad (6)$$

The integration takes place along a closed loop in the compactified imaginary time  $\tau \equiv x_4$ , where  $\mathcal{A}_4 = i\mathcal{A}_0$  is the matrix-valued temporal component of the Euclidean gauge field  $\mathcal{A}_\mu$  and the symbol  $\mathcal{P}$  denotes path ordering that insures the gauge-covariance of the whole expression (6). In the PLSM<sub>q</sub>, the Polyakov loop  $L$  plays the role of a homogeneous classical scalar field, which can be associated with a coordinate-independent gluon field  $\mathcal{A}_4 = t_3 \mathcal{A}_4^{(3)} + t_8 \mathcal{A}_4^{(8)}$  as  $\Phi = \exp(i\mathcal{A}_4/T)$ , where  $t_3$  and  $t_8$  are the diagonal generators of the  $SU(3)$  gauge group.

The Polyakov loop serves as an approximate order parameter for the confining properties of QCD. The expectation value of the Polyakov loop (6) vanishes at zero temperature, signaling the absence of the free quarks at  $T = 0$  and taking a finite value at the high temperature in the quark-gluon plasma phase. The confining properties of the two phases are also smoothly connected. In a pure Yang-Mills theory (in the limit of QCD when the masses of quarks become infinitely large), the Polyakov loop becomes an exact order parameter that vanishes (is a finite quantity) in the whole low-temperature (high-temperature) phase. The Lagrangian of the theory is invariant under the center  $\mathbb{Z}_3$  symmetry,  $L \rightarrow e^{2\pi ni/3} L$ , with  $n = 0, 1, 2$ , which is pertinent to the pure gauge theory. At the same time, a coupling to dynamical quarks breaks the  $\mathbb{Z}_3$  symmetry explicitly.

The Polyakov loop is coupled to the rest of the fields in the linear sigma model, similar to the case of the Nambu–Jona-Lasinio model as discussed in Refs. [31, 32, 40]. The second term in Eq. (1),

$$\mathcal{L}_L = -V_L(L, T), \quad (7)$$

is the potential term of the Polyakov action in the pure Yang-Mills theory not coupled to quarks. We treat the Polyakov loop in a mean-field approach, disregarding a kinetic term for this variable.

We use a specific form for the phenomenological potential of the Polyakov loop [40]:

$$\frac{V_L(L, T)}{T^4} = -\frac{1}{2} a(T) L^* L \quad (8)$$

$$+ b(T) \ln \left[ 1 - 6 L^* L + 4 \left( L^{*3} + L^3 \right) - 3 \left( L^* L \right)^2 \right],$$

with the parameters

$$a(T) = a_0 + a_1 \left( \frac{T_0}{T} \right) + a_2 \left( \frac{T_0}{T} \right)^2, \quad (9a)$$

$$b(T) = b_3 \left( \frac{T_0}{T} \right)^3, \quad (9b)$$

where  $T_0$  is the critical temperature in the pure gauge case:  $T_0 \equiv T_{SU(3)} = 270$  MeV. The phenomenological parameters in Eq. (9) are

$$a_0 = 16 \pi^2 / 45 \approx 3.51, \quad a_1 = -2.47, \quad (10)$$

$$a_2 = 15.2, \quad b_3 = -1.75.$$

The set of parameters (10) satisfies, with reasonable accuracy, the following requirements emergent from thermodynamics of  $SU(3)$  Yang-Mills theory [40]: (i) the Stefan-Boltzmann limit is reached at  $T \rightarrow \infty$ ; (ii) a first-order phase transition takes place at  $T = T_0$ ; (iii) the potential describes the existing lattice data for the Polyakov loop and the thermodynamic functions such as pressure, energy density, and entropy.

Definition (6) of the Polyakov loop implies that the value of this quantity is limited to the interval  $|L^*| \leq 1$  and  $|L| \leq 1$ , which is also consistent with a logarithmic divergence of the potential (8). According to the parameter set (10), the value  $L^* = L = 1$  can only be reached in the limit  $T \rightarrow \infty$ . In the confined phase,  $T < T_0$ , the potential has one trivial minimum,  $L = 0$ . As the temperature rises and the system undergoes the phase transition, the single minimum at  $L = 0$  of the potential splits into three degenerate minima labeled by the  $\mathbb{Z}_3$  variable. Thus, in the deconfined phase, the  $\mathbb{Z}_3$  symmetry is spontaneously broken, and  $\langle L \rangle \neq 0$ .

## 3. Quark sector

The third term of the full Lagrangian (1),

$$\mathcal{L}_q = \bar{\psi} [i\mathcal{D} - g(\sigma + i\gamma_5 \vec{\tau} \cdot \vec{\pi})] \psi, \quad (11)$$

describes the spinor doublet  $\psi = (u, d)^T$  of the light quarks which interacts with the meson fields  $\sigma$  and  $\vec{\pi}$ . The spinor field  $\psi$  also interacts with the  $SU(3)$  gauge field  $A_\mu$  via the covariant derivative:

$$\mathcal{D} = \gamma^\mu D_\mu, \quad D_\mu = \partial_\mu - i\mathcal{A}_\mu. \quad (12)$$

The gauge field represents, according to Eq. (6), a non-trivial background due to the Polyakov loop  $L$ .

The spontaneous symmetry breaking in the chiral field sector,  $\langle\sigma\rangle \neq 0$ , also gives the constituent mass  $m_q \equiv g\langle\sigma\rangle$  to the quark field. Setting the vacuum mass for the constituent quark to 307 MeV gives us the Yukawa coupling  $g \simeq 3.3$ . At low temperatures, quarks are not excited, and the model (2) becomes the standard linear  $\sigma$ -model without quarks [41].

Thus, the fermion field  $\psi$  couples two other variables: the Polyakov loop  $L$  and the chiral field  $\phi$ , linking confining and chiral properties together. Moreover, the dynamical quark fields  $\psi$  are affected by the global rotation. As the quarks interact with the Polyakov loop  $L$  and the chiral field  $\phi$ , the rotation influences both the chiral dynamics and the confining properties of the model. Therefore, this model allows us to study how rotating simultaneously affects color confinement and chiral symmetry breaking.

## B. Thermodynamics of nonrotating system

Before considering the main subject of our paper, the quark system in rotation, we first describe comprehensively a general principle how the thermodynamics of the non-rotating plasma determined in the PLSM $_q$  model. A more detailed review and careful determination of the thermodynamical properties of the model will be reported in our forthcoming paper [42].

### 1. Thermodynamic potential

We adopted the mean-field approximation by replacing  $\sigma$  and  $\vec{\pi}$  by their mean-field (expectation) values. As we discussed above, in the ground state,  $\langle\vec{\pi}\rangle \equiv 0$  in all studied phases. The quantity  $\langle\sigma\rangle$  determines the strength of the chiral symmetry breaking and can be nonzero.

The partition function of the PLSM $_q$  follows directly from its Lagrangian (1):

$$\mathcal{Z} = \exp\left\{-\frac{V_{3d}}{T} [V_\phi(\sigma, \vec{\pi}) + V_L(L)]\right\} \times \int \mathcal{D}\psi \mathcal{D}\bar{\psi} \exp\left\{-\int_0^\beta d\tau \int_V d^3x \mathcal{L}_q(\psi, \sigma, L)\right\}, \quad (13)$$

where an irrelevant overall normalization factor has been omitted. Equation (13) gives us the thermodynamic potential of the model,

$$F(T) \equiv -\frac{T \ln \mathcal{Z}}{V} = V_\phi(\sigma) + V_L(L) + F_{\psi\bar{\psi}}(\sigma, L), \quad (14)$$

where the meson potential  $V_\phi$  and the Polyakov loop potential  $V_L$  can be read from Eqs. (3) and (8).

The last term in Eq. (14) corresponds to the quark contribution to the thermodynamic potential, which is

given by the last multiplier in Eq. (13). The quark part can be split into its vacuum and thermal constituents:  $F_{\psi\bar{\psi}} = F_{\psi\bar{\psi}}^{\text{vac}} + F_{\psi\bar{\psi}}^\beta$ , where the vacuum contribution to the free energy,

$$F_{\psi\bar{\psi}}^{\text{vac}} = -2N_c N_f \int \frac{d^3p}{(2\pi)^3} E, \quad (15)$$

is infinite. We, however, follow the arguments provided in Ref. [36] and ignore below the vacuum quark part by setting  $F_{\psi\bar{\psi}}^{\text{vac}} = 0$ . Since now  $F_{\psi\bar{\psi}} = F_{\psi\bar{\psi}}^\beta$ , we will omit the ‘‘thermal’’  $\beta$  superscript and instead identify the fermionic free energy entirely with its thermal contribution [36, 43]:

$$F_{\psi\bar{\psi}} = -2N_f T \int \frac{d^3p}{(2\pi)^3} \sum_{\zeta=\pm} \text{Tr}_c \ln \left[ 1 + e^{-\beta(\mathcal{E}_\zeta + i\zeta A_4)} \right], \quad (16)$$

where  $\mathcal{E}_\zeta = E - \zeta\mu$  represents the effective energy relative to the Fermi level  $E_F = \mu$  for particles ( $\zeta = +$ ) and  $E_F = -\mu$  for antiparticles ( $\zeta = -$ ), with  $\mu$  being the quark chemical potential. The trace  $\text{Tr}_c$  over colour indices can be taken explicitly:

$$F_{\psi\bar{\psi}} = -2N_f T \sum_{\zeta=\pm 1} \int \frac{d^3p}{(2\pi)^3} F_\zeta, \quad (17)$$

where we introduced the particle and antiparticle free energies, respectively (see Ref. [44] for technical details):

$$F_+ = \ln \left[ 1 + 3L e^{-\beta\mathcal{E}_+} + 3L^* e^{-2\beta\mathcal{E}_+} + e^{-3\beta\mathcal{E}_+} \right], \\ F_- = \ln \left[ 1 + 3L^* e^{-\beta\mathcal{E}_-} + 3L e^{-2\beta\mathcal{E}_-} + e^{-3\beta\mathcal{E}_-} \right]. \quad (18)$$

### 2. Saddle point approximation

We find the mean-field values of the fields  $\sigma$  and  $L$  at thermodynamic equilibrium by minimizing the total free energy with respect to  $\sigma$ ,  $L_+ \equiv L$ , and  $L_- \equiv L^*$  variables:

$$\frac{\partial F}{\partial \sigma} = \frac{\partial F}{\partial L} = \frac{\partial F}{\partial L^*} = 0. \quad (19)$$

These equations can be expressed with the help of the following derivatives:

$$f_{\pm} = -\frac{1}{3} \frac{\partial F_{\pm}}{\partial(\beta\mathcal{E}_{\pm})}, \quad f_{\pm,+} = \frac{1}{3} \frac{\partial F_{\pm}}{\partial L_+}, \quad f_{\pm,-} = \frac{1}{3} \frac{\partial F_{\pm}}{\partial L_-}, \quad (20)$$

From Eq. (18), it is not difficult to see that the above quantities take the following explicit form:

$$f_{\pm} = \frac{L_{\pm} e^{-\beta\mathcal{E}_{\pm}} + 2L_{\mp} e^{-2\beta\mathcal{E}_{\pm}} + e^{-3\beta\mathcal{E}_{\pm}}}{1 + 3L_{\pm} e^{-\beta\mathcal{E}_{\pm}} + 3L_{\mp} e^{-2\beta\mathcal{E}_{\pm}} + e^{-3\beta\mathcal{E}_{\pm}}}, \quad (21a)$$

$$f_{\pm,\pm} = \frac{e^{-\beta\mathcal{E}_{\pm}}}{1 + 3L_{\pm} e^{-\beta\mathcal{E}_{\pm}} + 3L_{\mp} e^{-2\beta\mathcal{E}_{\pm}} + e^{-3\beta\mathcal{E}_{\pm}}}, \quad (21b)$$

$$f_{\pm,\mp} = \frac{e^{-2\beta\mathcal{E}_{\pm}}}{1 + 3L_{\pm} e^{-\beta\mathcal{E}_{\pm}} + 3L_{\mp} e^{-2\beta\mathcal{E}_{\pm}} + e^{-3\beta\mathcal{E}_{\pm}}}. \quad (21c)$$

One obtains the following explicit form of the saddle-point equations (19):

$$\frac{\partial F}{\partial \sigma} = \frac{\partial V_\phi}{\partial \sigma} + g\langle\bar{\psi}\psi\rangle, \quad (22)$$

$$\frac{\partial F}{\partial L_\pm} = \frac{\partial V_L}{\partial L_\pm} - 6N_f T \sum_{\varsigma=\pm 1} \int \frac{d^3 p}{(2\pi)^3} f_{\varsigma,\pm}, \quad (23)$$

where we identified the fermion condensate in the first equation,

$$\langle\bar{\psi}\psi\rangle = 6N_f g\sigma \sum_{\varsigma=\pm 1} \int \frac{d^3 p}{(2\pi)^3 E} f_\varsigma, \quad (24)$$

while the derivatives of the mesonic and Polyakov loop potentials read as follows:

$$\frac{\partial V_\phi}{\partial \sigma} = \lambda(\sigma^2 - v^2)\sigma - h, \quad (25a)$$

$$\begin{aligned} \frac{\partial V_L}{\partial L_\pm} = & -\frac{6T^4 b(T)(L_\mp - 2L_\pm^2 + L_\pm^2 L_\mp)}{1 - 6L^* L + 4(L^{*3} + L^3) - 3(L^* L)^2} \\ & - \frac{T^4}{2} a(T) L_\mp. \end{aligned} \quad (25b)$$

One immediately notices that Eqs. (25) contain cubic powers of the order parameters, which implies that the saddle-point equations (19) should provide us with multiple solutions. The physically permitted solutions should satisfy the following constraints:

$$0 < \sigma \leq f_\pi, \quad 0 \leq L, L^* < 1. \quad (26)$$

The first condition in Eq. (26) appears on physical grounds as we expect that both thermal fluctuations and finite-density environment restore the chiral symmetry instead of enhancing its breaking. This assertion is equivalent to the statement that the zero-temperature QCD vacuum, defined as a state at  $T = 0$  and  $\mu = 0$  (and, appropriately, at  $\Omega = 0$ ), the highest value of the mean-field (expectation) value of the  $\sigma$  meson field gives the quarks their maximal (constituent) dynamical mass,  $m_q = g\sigma$ , in the whole phase diagram. The value of  $\sigma$  is a positive quantity because of the presence of the last term in the potential (3) on the chiral field  $\phi$ , with  $h > 0$  fixed by the phenomenology.

The second restriction in Eq. (26) also has two bounds. The lower bound appears due to the property that in the vacuum, the Polyakov loop expectation value vanishes,  $L = L^* = 0$ , reflecting the fact that the addition of an infinitely heavy (anti-)quark requires an infinitely large change in the free energy of the system. Therefore, the corresponding free energies, of quark,  $F_Q = -T \ln L$ , and of an anti-quark,  $F_{\bar{Q}} = -T \ln L^*$ , are infinite. Notice that within the scope of the Polyakov loop models, the two conjugate fields  $L$  and  $L^*$  are treated as real but independent numbers. It means, in particular, that the free energy of a heavy (anti-)quark, defined above, is a real number.

As the medium becomes more energetic (either denser, at higher chemical potential  $\mu$ ; or hotter, at higher temperature  $T$ ), the quark-gluon medium enters a deep deconfinement phase, which is achieved when the Polyakov loop approaches its maximal expectation value of  $L, L^* \rightarrow 1$ . Values outside the intervals indicated in Eq. (26) cannot represent physically realizable systems. The upper bound on the Polyakov loop (26) arises due to the mathematical definition of the Polyakov loop (6).

Moreover, if even Eqs. (19) give us multiple solutions satisfying the physical constraints of Eqs. (26), we should select the true ground state distinguishing it from unstable and (meta)stable states. The unstable solutions correspond to points of, respectively, local maxima or saddle points of the total free energy,  $F$ . The lowest-free-energy minimum represents the true stable ground state of the system. Quantum and thermal fluctuations typically drive a quantum system from metastable states, associated with local free energy minima, to the true ground state, corresponding to its global minimum.

In order to evaluate the free energy (14), we add the mesonic potential (3) and the Polyakov-loop potential (8) to the fermionic contribution (16). The latter expression can be simplified using the integration by parts,

$$F_{\psi\bar{\psi}} \equiv -P_{\psi\bar{\psi}} = -6N_f \sum_{\varsigma=\pm 1} \int \frac{d^3 p}{(2\pi)^3} \frac{p^2}{3E} f_\varsigma. \quad (27)$$

In consistency with thermodynamics of fermionic gases, the fermionic pressure (27) is given by the expectation value of the canonical expression:  $P_{\psi\bar{\psi}} = -\frac{i}{6} \bar{\psi} \gamma \cdot \vec{\nabla} \psi$ .

### C. Phase diagram of non-rotating plasma

For a static plasma, the thermodynamic limit has a well-defined meaning, which allows us to check our algorithms for determining the phase diagram before proceeding, in the next section, to the more complicated case of rigidly rotating plasma.

In terms of the chiral properties, the phase diagram of the theory contains two phases: the chirally broken phase and the chirally restored phase, separated by a transition point. At low values of the vector chemical potential, the phase diagram is known to possess a smooth crossover, which does not contain any thermodynamic singularity. Therefore, both phases are analytically connected. At higher values of the chemical potential, the division between the phases turns into a first-order phase transition separated from crossover by an end-point at which the system experiences a second-order phase transition.

A similar behavior is also pertinent to the Polyakov loop expectation value, which is an order parameter for the confining (low-temperature) and deconfining (high-temperature) phases. Below, we demonstrate these properties, highlighting the subtleties of the determination of the critical points in the phase diagram.

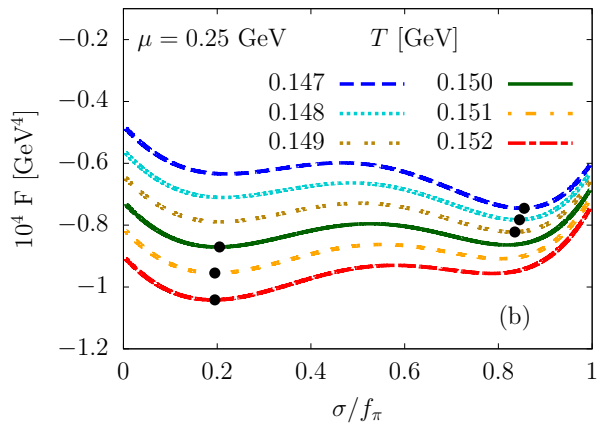


FIG. 1. Dependence of the grand canonical potential  $F$  in the  $\text{PLSM}_q$  model on the expectation value of the  $\sigma$  field at the fixed value of the vector chemical potential,  $\mu = 0.25$  GeV. Various temperatures near the phase transition point are shown. The small filled circles indicate the value of the normalized expectation value of the sigma field,  $\sigma/f_\pi$ , which corresponds to the global minimum of  $F$  at each temperature  $T$ .

Figure 1 illustrates a typical behavior of the full thermodynamic potential (14) – excluding the vacuum part – as a function of the  $\sigma$  mean field at the vector chemical potential  $\mu = 0.25$  GeV, which is sufficiently large to allow for a first-order phase transition. In this figure, we consider the field  $\sigma$  as a free (external) parameter and find the values of the  $L$  and  $L^*$  that minimize  $F$  at the fixed values of  $\sigma$ ,  $T$ , and  $\mu$ . In the vicinity of the phase transition, the free energy  $F$  develops multiple extrema corresponding to two minima and one maximum. The thermodynamically favored phase corresponds to the global minimum, while the other minimum represents a metastable state and the maximum gives us an unstable point.

At this particular value of the vector chemical potential,  $\mu = 0.25$  GeV, the phase transition appears at  $T_c \simeq 0.15$  GeV, implying that the theory stays in the chirally-broken phase at lower temperatures and in the chirally-restored phase at higher temperatures. Notice that the chiral restoration in the high-temperature phase has an approximate meaning because both these phases are analytically connected. Indeed, Fig. 1 shows that at the phase transition point, the mean value of the field  $\sigma$  drops rather strongly but still does not vanish at the high-temperature phase at  $T > T_c$ . The same remark applies also to the deconfinement transition.

Figure 2 shows the order parameter for the chiral transition,  $\sigma$ , normalized to its vacuum value  $\sigma_{\text{vac}} = f_\pi$  as a function of temperature. In the same figure, we also show the expectation value of the Polyakov loop, which is the confinement order parameter. This figure clearly shows that the increase in temperature or chemical potential drives the system from the confinement (chirally broken) to the deconfinement (chirally restored) phase, as expected.

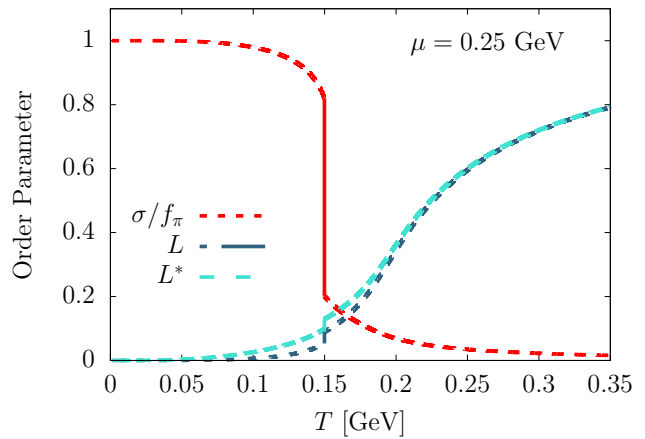


FIG. 2. Temperature dependence of the normalized order parameter for the chiral phase transition,  $\sigma/f_\pi$ , and the order parameters for the confinement-deconfinement transitions,  $L$  and  $L^*$ , at  $\mu = 0.25$  GeV.

Notice that the presence of finite density of quark matter, characterized by the non-zero chemical potential,  $\mu \neq 0$ , leads to the explicit breaking of the charge-conjugation symmetry. In other words, the properties of quarks become different from the properties of anti-quarks. In particular, the free energy of an infinitely heavy quark,  $F_Q = -T \ln L$ , and the free energy of an anti-quark,  $F_{\bar{Q}} = -T \ln L^*$ , differ from each other (we remind that both  $L$  and  $L^*$  are real-valued quantities). Figure 2 illustrates this behavior: adding another quark to a quark-rich medium (with  $\mu > 0$ ) is more costly than adding an anti-quark to the same medium (in other words,  $F_Q > F_{\bar{Q}}$  for all values of  $\mu > 0$ ).

We are now interested in identifying a line in the  $(T-\mu)$  plane of parameters where exactly the transition takes place. In the case of a first-order phase transition, which is realized in the presence of a nonzero quark density, it is sufficient to find the point along the temperature direction (that is, at a fixed  $\mu$  and varying  $T$ ) where the order parameter(s) exhibit a discontinuity. Typically, the discontinuity in the  $\sigma$  condensate is accompanied by discontinuities in the other thermodynamic parameters, including in the values of the Polyakov loops  $L$  and  $L^*$ . While the intuitive picture of the (phase) transition behavior is clearly seen from Fig. 2 at a high  $\mu$ , it is not the case at lower densities, where the system undergoes a so-called crossover transition without encountering a thermodynamic singularity.

In the absence of a discontinuity at low  $\mu$ 's, the system goes continuously from one phase to the other as parameters change. In practical terms, discrimination between a first-order transition and a sharp crossover transition poses a formidable numerical challenge. Pinpointing the exact position of the pseudo-critical parameters of the crossover transition has a certain degree of arbitrariness, which depends on the choice of the observables used to identify the crossover.

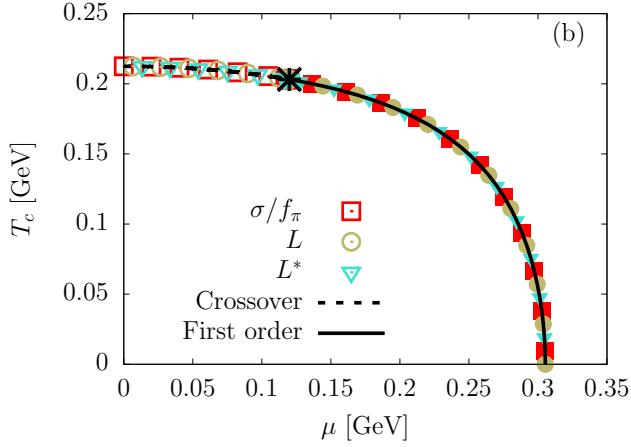


FIG. 3. Phase diagram for unbounded static PLSM<sub>q</sub> model in  $T - \mu$  plane for the normalized order parameter of the chiral transition  $\sigma/f_\pi$ , as well as the confining transition,  $L$  and  $L^*$ . The phase diagram features a crossover transition line at lower vector chemical potentials  $\mu$ , which is marked by the dashed line. The first-order phase transition at higher values of  $\mu$  is shown by the solid line. The critical end-point that separates these regimes occurs at  $(T_c, \mu_c) = (0.2043, 0.1123)$  GeV. It is marked by the star “\*”.

In our work, the point of the crossover is identified as an inflection point with respect to the relevant order parameter  $\sigma$ ,  $L$ , and  $L^*$ . The inflection is searched along a straight line that is connected with the origin of the parameter space,  $\mu = T = 0$ . The resulting phase diagram is shown in Fig. 3. Qualitatively, it agrees with known results obtained in the thermodynamic limit [19].<sup>1</sup> There is no splitting between the deconfining and chirality-restoring transitions neither for thermodynamic phase transition at higher  $\mu$  nor for the crossover regime at the lower-density part of the phase diagram at smaller values of the chemical potential  $\mu$ . As we will see below, this property will be lost for a system where two of the three spatial directions are bounded, as it is pertinent to the rotating systems.

### III. THE PLSM<sub>q</sub> MODEL IN RIGID ROTATION

Below, we discuss the formulation of the PLSM<sub>q</sub> system at finite angular momentum. To facilitate the analysis of the phase diagram, we will employ corotating coordinates, defined by the angular velocity  $\Omega$  entering the grand canonical ensemble. To avoid superluminal corotating velocities, the system must be enclosed in a cylindrical volume, where suitable boundary conditions must

be enforced in the plane transverse to the angular velocity vector.

#### A. Co-rotating frame

The description of the fermionic fields in the corotating reference frame follows the standard procedure [20, 46, 47]. We switch to corotating coordinates, defined with respect to the static cylindrical coordinates of the inertial laboratory reference frame (denoted by subscript “lab”) by

$$t = t_{\text{lab}}, \quad \varphi = \varphi_{\text{lab}} - \Omega t_{\text{lab}}, \quad (28)$$

where  $\Omega \equiv |\Omega| > 0$  represents the angular frequency of the corotating observer. The line element  $ds^2 = g_{\mu\nu} dx^\mu dx^\nu$  in the corotating coordinates reads as follows:

$$ds^2 = (1 - \rho^2 \Omega^2) dt^2 - 2\rho^2 \Omega dt d\varphi - d\rho^2 - \rho^2 d\varphi^2 - dz^2. \quad (29)$$

According to the standard procedure, the curvilinear metric  $g_{\mu\nu}$  can be brought to Minkowski form by introducing the non-holonomic, orthonormal tetrad (vierbein) vector field,  $e_{\hat{\alpha}} = e_{\hat{\alpha}}^\mu \partial_\mu$ , and the associated one-forms  $\omega^{\hat{\alpha}} = \omega_{\hat{\alpha}}^\mu dx^\mu$ , defined by

$$\begin{aligned} e_{\hat{t}} &= \partial_t - \Omega(y\partial_x - x\partial_y), & \omega^{\hat{t}} &= dt, \\ e_{\hat{x}} &= \partial_x, & \omega^{\hat{x}} &= dx + \Omega y dt, \\ e_{\hat{y}} &= \partial_y, & \omega^{\hat{y}} &= dy - \Omega x dt, \\ e_{\hat{z}} &= \partial_z, & \omega^{\hat{z}} &= dz, \end{aligned} \quad (30)$$

such that  $g_{\mu\nu} = \eta_{\hat{\alpha}\hat{\beta}} \omega_{\hat{\alpha}}^\mu \omega_{\hat{\beta}}^\nu$  and  $\omega_{\hat{\alpha}}^\mu e_{\hat{\beta}}^\mu = \delta_{\hat{\alpha}\hat{\beta}}$ .

The Cartan coefficients associated with the tetrad are defined by the commutation relation  $[e_{\hat{\alpha}}, e_{\hat{\rho}}] = c_{\hat{\alpha}\hat{\rho}}^{\hat{\sigma}} e_{\hat{\sigma}}$ , where  $e_{\hat{\alpha}}$  are considered as differential operators (30). Taking into account the following explicit form of the nontrivial pairs of these commutation relations,

$$[e_{\hat{t}}, e_{\hat{x}}] = e_{\hat{y}}, \quad [e_{\hat{t}}, e_{\hat{y}}] = -e_{\hat{x}}, \quad (31)$$

we find the following non-vanishing Cartan coefficients:

$$c_{\hat{t}\hat{x}}^{\hat{y}} = c_{\hat{t}\hat{y}}^{\hat{x}} = \Omega. \quad (32)$$

The connection coefficients  $\Gamma_{\hat{\rho}\hat{\sigma}\hat{\alpha}} = \frac{1}{2}(c_{\hat{\rho}\hat{\sigma}\hat{\alpha}} + c_{\hat{\rho}\hat{\sigma}\hat{\alpha}} - c_{\hat{\rho}\hat{\sigma}\hat{\alpha}})$  vanish identically, except for the following component:

$$\Gamma_{\hat{x}\hat{y}\hat{t}} = -\Omega. \quad (33)$$

The Dirac action can be written in curvilinear coordinates as

$$\begin{aligned} S &= \int d^4x \sqrt{-g} \mathcal{L}_D, \\ \mathcal{L}_D &= \bar{\psi} [i\mathcal{D} + \mathcal{A} + \mu\gamma^0 - g\sigma] \psi, \end{aligned} \quad (34)$$

where  $D_\mu = \partial_\mu - \Gamma_\mu$  is the covariant derivative and  $\mathcal{A} = \gamma^\mu \mathcal{A}_\mu$  is the Abelian gauge field, corresponding to

<sup>1</sup> The predictions of the effective models may differ quantitatively depending on number quark flavors, values of the model couplings, treatment of field fluctuations and implementation of renormalization, (see, for example, Ref. [45]).

the Cartan subgroup of the  $SU(3)$  gauge group, written in the Feynman slash notation. Here, we have also included the vector chemical potential  $\mu$  to account for the shifts of the Dirac sea in the presence of matter–anti-matter imbalance. The spin connection coefficient is given by  $\Gamma_\mu = -\frac{i}{2}\omega_\mu^{\hat{\alpha}}\Gamma_{\hat{\beta}\hat{\gamma}\hat{\alpha}}S^{\hat{\beta}\hat{\gamma}}$ , where the structure  $S^{\hat{\beta}\hat{\gamma}} = \frac{i}{4}[\gamma^{\hat{\beta}}, \gamma^{\hat{\gamma}}]$  represent the spin part of the generators of the Lorentz transformations.

We choose the gamma matrices with respect to the tetrad vector fields in the Dirac representation,

$$\gamma^{\hat{t}} = \begin{pmatrix} 1 & 0 \\ 0 & -1 \end{pmatrix}, \quad \gamma^{\hat{i}} = \begin{pmatrix} 0 & \sigma^i \\ -\sigma^i & 0 \end{pmatrix}, \quad (35)$$

with  $\sigma^{\hat{i}}$  being the Pauli spin matrices:

$$\sigma^{\hat{x}} = \begin{pmatrix} 0 & 1 \\ 1 & 0 \end{pmatrix}, \quad \sigma^{\hat{y}} = \begin{pmatrix} 0 & -i \\ i & 0 \end{pmatrix}, \quad \sigma^{\hat{z}} = \begin{pmatrix} 1 & 0 \\ 0 & -1 \end{pmatrix}. \quad (36)$$

With the above convention, the single non-vanishing spin connection coefficient takes the simple form,  $\Gamma_{\hat{t}} = i\Omega S^z$ , implying

$$iD_{\hat{t}} = i\partial_t + \Omega J^z, \quad (37)$$

where

$$J^z = -i\partial_\varphi + S^z, \quad S^z = \frac{1}{2} \begin{pmatrix} \sigma^z & 0 \\ 0 & \sigma^z \end{pmatrix}, \quad (38)$$

are the operators of the total angular momentum and its spin part, respectively.

Then, the Dirac equation for the spinor  $\psi$  in the co-rotating reference frame reads as follows:

$$[\gamma^0(i\partial_t + \mathcal{A}_0 + \mu + \Omega J^z) + i\boldsymbol{\gamma} \cdot \boldsymbol{\nabla} - g\sigma]\psi = 0. \quad (39)$$

Its charge conjugate that satisfies the same equation is

$$\psi^c = i\gamma^2\psi^* \Big|_{\mathcal{A}^\mu \rightarrow -\mathcal{A}^\mu, \mu \rightarrow -\mu}. \quad (40)$$

The Dirac equation in the rotating reference frame (39) implies a simple linear relation,

$$H = H_{\text{lab}} - \boldsymbol{\Omega} \cdot \boldsymbol{J}, \quad (41)$$

between the Dirac Hamiltonian in the rotating reference frame,  $H = i\partial_t$ , and the Hamiltonian in the laboratory reference frame,  $H_{\text{lab}} = i\partial_{t_{\text{lab}}}$ . The change in the Hamiltonian of the system (41) as we move from one reference system to the other is given by the coupling of the angular velocity  $\boldsymbol{\Omega}$  and the total angular momentum  $\boldsymbol{J}$ . The same property applies also to classical mechanical systems and to thermodynamics [48, 49].

Below, the thermodynamic quantities will be evaluated in the Euclidean spacetime in the Matsubara formalism. Under the Wick rotation to the imaginary time,  $t \rightarrow \tau = it$ , the partition function of the model gets the form:

$$Z = \int [id\psi^\dagger][d\psi] \exp(S_E), \\ S_E = \int_0^\beta d\tau \int_V d^3x \mathcal{L}_E, \quad (42)$$

where  $V$  represents the system volume (a cylinder of radius  $R$  and infinite longitudinal extent). The Euclidean Lagrangian  $\mathcal{L}_E$  reads as follows:

$$\mathcal{L}_E = \bar{\psi} [\gamma^0(-\partial_\tau + \Omega J^z + i\mathcal{A}_4 + \mu) + i\boldsymbol{\gamma} \cdot \boldsymbol{\nabla} - g\sigma] \psi. \quad (43)$$

## B. Dirac modes and spectral boundaries

In order to understand the thermodynamics of the rotating system, we need to calculate the eigenenergy of the Hamiltonian  $H = i\partial_t$  in the rotating reference frame, which is bound in the transverse directions by a cylindrical boundary. The eigenvalues are characterized by the quantum numbers associated with the angular momentum  $J^z$ , the longitudinal momentum  $P^z = -i\partial_z$ , and the helicity  $h = \mathbf{S} \cdot \mathbf{P}/p$  operators. These operators commute with the Hamiltonian, and therefore, their eigenvalues can be used to label the system solutions. The solution can be found using the strategy of Ref. [50] generalized to the  $N_f = 2$  flavor fermions in the constant Polyakov loop background with  $N_c = 3$  colors. Omitting the technical details that will be presented elsewhere [42], we outline briefly below the most essential features of this procedure.

Using the cumulative label  $j$  to denote the eigenvalues, we impose

$$HU_j = \tilde{\omega}_j^a U_j, \quad J^z U_j = m_j U_j, \\ P^z U_j = k_j U_j, \quad hU_j = \lambda_j U_j. \quad (44)$$

Here the frequency  $\tilde{\omega}_j^a$  is related to the Minkowski energy  $E_j > 0$  in the laboratory reference frame as follows:

$$\tilde{\omega}_j^a = \varsigma_j E_j - \mathcal{A}_{0;j} - \mu - \Omega m_j. \quad (45)$$

The right-hand side corresponds to a solution of the Dirac equation (39) for which the symbol  $\varsigma_j = \pm 1$  distinguishes between particle (positive energy) and anti-particle (negative energy) solutions. The superscript  $a$  indicates that the gauge field contribution corresponding to the Polyakov-loop background has been taken into account,  $\tilde{\omega}_j^a = \tilde{\omega}_j - \mathcal{A}_{0;j}$ . The tilde notation denotes the subtraction of the angular momentum term,  $\tilde{\omega}_j = \omega_j - \Omega m_j$ , corresponding to the shift in the Hamiltonian (41), while  $\omega_j = \varsigma_j E_j - \mu$ . Notice that the index  $m_j$  runs over half-integer numbers,  $m_j = \pm 1/2, \pm 3/2, \dots$

In the mean-field approximation that we are employing, the gauge field is diagonal in color space,  $\mathcal{A}_0 = \frac{1}{2}(A_0^3 t^3 + A_0^8 t^8)$ . The cylindrical modes  $U_j$  in Eq. (44) can be taken as eigenvectors of both diagonal generators  $t^3$  and  $t^8$  of the gauge  $SU(3)$  group. Thus,

$$\mathcal{A}_0 U_j = \mathcal{A}_{0;j} U_j, \quad (46)$$

where we denote the components of the background field



$$(A_{0;1}, A_{0;2}, A_{0;3}) = (\phi, \phi', -\phi - \phi'),$$

$$\begin{aligned}\phi &= \frac{1}{2}A_0^3 + \frac{1}{2\sqrt{3}}A_0^8, \\ \phi' &= -\frac{1}{2}A_0^3 + \frac{1}{2\sqrt{3}}A_0^8, \\ -\phi - \phi' &= -\frac{1}{\sqrt{3}}A_0^8,\end{aligned}\quad (47)$$

of the SU(3) Polyakov loop:

$$L_+ \equiv L = \frac{1}{3}(e^{i\phi} + e^{i\phi'} + e^{-i\phi - i\phi'}), \quad (48)$$

$$L_- \equiv L^* = \frac{1}{3}(e^{-i\phi} + e^{-i\phi'} + e^{i\phi + i\phi'}). \quad (49)$$

The modes  $U_j$  must satisfy boundary conditions on the enclosing cylinder of radius  $R$ . In this paper, we employ the spectral boundary conditions [51] as discussed for the cylindrical setup in Ref. [50]. These conditions provide necessary and sufficient conditions to yield a consistent quantization by requiring the self-adjointness of the Hamiltonian. In terms of the eigenspinors  $U_j$ , the spectral condition amounts to the vanishing of either the top and third (for  $m > 0$ ) or the second and fourth components of the spinor  $U_j$  (for  $m < 0$ ). These conditions guarantee the conservation of the total vector (baryon) charge inside the cylinder, as well as the self-adjointness of the Hamiltonian.

The solutions of the eigenvalue equations (44) for a single-species fermion satisfying the spectral boundary conditions were reported in Ref. [50]. For our problem, the eigenenergies are given by Eq. (45), where  $E_j = \sqrt{p_j^2 + M^2}$  is the Minkowski energy,  $M = g\sigma$  is the particle mass,  $p_j^2 = \sqrt{q_j^2 + k_j^2}$  is the total momentum magnitude and the transverse momentum  $q_j$  is quantized due to the imposed cylindrical boundary conditions:

$$q_j R = \begin{cases} \xi_{m_j - \frac{1}{2}, \ell_j}, & m_j > 0, \\ \xi_{-m_j - \frac{1}{2}, \ell_j}, & m_j < 0. \end{cases} \quad (50)$$

Here  $\xi_{n\ell}$  is the  $\ell$ th nonzero root of the Bessel function:

$$J_n(\xi_{n\ell}) = 0, \quad \text{with} \quad n \geq 0, \quad (51)$$

where the natural number  $l = 1, 2, \dots$  labels the radial modes.

The quantization is compatible with the charge conjugation operation, by which the spinors  $V_j(x) = i\gamma^2 U_j^*(x) = i(-1)^{m_j} \varsigma_j U_{\bar{j}}(x)$  must also belong to the set of the modes  $\{U_j\}$ . Here, the cumulative index  $\bar{j}$  represents the set of charge-conjugated eigenvalues with respect to  $j$ , i.e.

$$\begin{aligned}j &= (\varsigma_j, f_j, c_j, \lambda_j, m_j, \ell_j, k_j), \\ \bar{j} &= (-\varsigma_j, f_j, c_j, \lambda_j, -m_j, \ell_j, -k_j),\end{aligned}\quad (52)$$

with  $f_j = u, d$  and  $c_j = 1, 2, 3$  being the flavour and colour quantum numbers, respectively.

### C. Free energy of the rotating system

The average thermodynamic potential of the rotating fermionic ensemble can be split into a vacuum and a thermal part, similar to the static case considered above. The thermal part can be written in analogy with Eq. (27):

$$F_{\psi\bar{\psi}} = -\frac{2TN_f}{\pi R^2} \sum_{b, \varsigma = \pm 1} \int_{-\infty}^{\infty} \frac{dk}{2\pi} \tilde{F}_{\varsigma}, \quad (53)$$

where we introduced for notational brevity the sum over the radial quantum numbers,

$$\sum_b = \sum_{m=-\infty}^{\infty} \sum_{l=1}^{\infty}, \quad (54)$$

keeping in mind that the index  $m = \pm\frac{1}{2}, \pm\frac{3}{2}, \dots$  runs over all odd half-integer values.

In order to compute  $\tilde{F}_{\varsigma}$  in Eq. (53), we note the following relation:  $\varsigma_j \tilde{\omega}_j^a = E_j - \varsigma_j(\Omega m_j + \mu + A_{0;c})$ . Flipping the sign of  $m_j$  in the sum over ‘‘b’’ for the antiparticle sector (when  $\varsigma_j = -1$ ), we have  $\varsigma_j \tilde{\omega}_j^a \rightarrow \tilde{\mathcal{E}}_j - \varsigma_j A_{0;c_j}$ , with  $\tilde{\mathcal{E}}_j = \mathcal{E}_j - \Omega m_j$  being the corotating effective energy and  $\mathcal{E}_j = E_j - \varsigma_j \mu$ . Then,  $\tilde{F}_{\varsigma}$  can be computed using the colour eigenvalue Eqs. (46)–(47) as follows:

$$\begin{aligned}\tilde{F}_{\varsigma} &= \sum_{c=1}^3 \ln(1 + e^{-\beta(\tilde{\mathcal{E}}_c - \varsigma A_{0;c})}) \\ &= \ln[1 + L_{\varsigma} e^{-\beta\tilde{\mathcal{E}}_c} + L_{-\varsigma} e^{-2\beta\tilde{\mathcal{E}}_c} + e^{-3\beta\tilde{\mathcal{E}}_c}].\end{aligned}\quad (55)$$

Notice that  $\tilde{F}_{\varsigma}$  in Eq. (55) coincides with the one in Eq. (16) after replacing the laboratory-frame energy  $\mathcal{E}_{\varsigma}$  with the corotating energy,  $\tilde{\mathcal{E}}_{\varsigma}$ .

The thermal free energy  $F_{\psi\bar{\psi}}$  in Eq. (53) is identical to the one for the static reference frame (17) after replacing the integration with respect to the three-momentum via

$$\int \frac{d^3p}{(2\pi)^3} \rightarrow \frac{1}{\pi R^2} \sum_b \int \frac{dk}{2\pi}. \quad (56)$$

So far, in this section, we have only discussed the thermodynamics of the fermionic part of the model. The bosonic part is encoded in the classical condensate  $\sigma$ , which is not affected by rotation directly. The effect of rotation on the field  $\sigma$  appears only through the interaction with fermionic loops, which do feel the rotation directly, as we discussed in this section. Moreover, we treat the condensate  $\sigma$  in the homogeneous approximation that is used in most of the studies so far. Namely, the condensate is set to be a coordinate-independent quantity. While noticing that the homogeneous approximation allows us to compare our results with the results of other approaches, we acknowledge that the realistic rotating plasma should develop a radial inhomogeneity, which should become rather pronounced for fast rotation [12, 52, 53].

## IV. SPLITTING OF TRANSITIONS

In this section, we thoroughly evaluate the phase diagram of the PLSM<sub>q</sub> inside the cylindrical volume following our strategy described in Section III.

### A. Effect of cylindrical boundaries for static plasma

#### 1. Softening, shifting, and splitting of transitions

We minimize the free energy of the system enclosed in the cylindrical cavity, Eqs. (14) with the fermionic free energy given in Eq. (53). The latter quantity can only be evaluated with the use of extensive numerical methods since the sum over the radial excitations (54), provided by the zeros of Bessel functions (50), can involve up to  $10^5$  terms to guarantee the convergence of the sum.

First, we consider a non-rotating case with  $\Omega = 0$ . In Fig. 4, we show the mean values of the chiral condensate and the Polyakov loops as the functions of temperature for various radii  $R$  of the cylinder at chemical potentials  $\mu = 0$  and  $\mu = 0.25$  GeV. In an infinite volume and for the vanishing chemical potential,  $\mu = 0$ , the transition has the nature of the smooth crossover since no order parameters show anything similar to a critical behavior. At  $\mu = 0.25$  GeV, the  $R \rightarrow \infty$  transition is a strong first-order phase transition. What happens with these transitions when we decrease the radius of the cylinder  $R$ ?

First, we notice that the decrease of the radius leads to the softening of the transition seen in the behaviour of all order parameters and for all chemical potentials. This property agrees with our experience for a finite volume, for which – if the system is bounded in all three directions – the thermodynamic phase transition cannot be realized. Therefore, even a first-order phase transition (that takes place at higher chemical potential) is softened, becoming a crossover transition in a finite volume. An existing smooth crossover at zero chemical potential becomes even softer. A similar softening behavior of our system, for which only two dimensions out of three are restricted, is compatible with the mentioned finite-size softening effect.

The described softening of the transition temperature is most clearly seen for the condensate  $\sigma$  for the large chemical potential  $\mu = 0.25$  GeV. As the radius diminishes, the jump in the condensate diminishes and, at  $R = 2$  fm, is not seen at all. This radius corresponds to the energy scale in 100 MeV, which is compatible with the pion mass. Therefore, the restriction of one of the dimensions to this value leads to a drastic softening effect on the phase transition.

Second, we find that the decrease in the radius of the cylinder  $R$  leads to an increase in the pseudocritical temperatures of both crossovers. This effect can also be anticipated given the fact that the decrease of the radius leads to an enhancement of the thermal contribution to the chiral condensate inside the cylinder [50]. In order

to break a stronger chiral condensate, higher temperatures are needed. Due to the coupling between the chiral and confining degrees of freedom in the PLSM<sub>q</sub>, the expectation value of the Polyakov loop follows the same behavior. The enhancement of the critical temperature is, therefore, a finite-volume phenomenon.

Third, we see that the inflection points at the smallest studied radius  $R = 1$  fm of the  $\sigma$  condensate and the mean Polyakov loop do not coincide, with the deconfinement crossover transition being slightly lower than the chiral transition. Therefore, one expects that in a system with bounded spatial dimensions, the chiral and confinement transitions split, thus creating an already-deconfined but still-chirally broken quark-gluon matter.

Strictly speaking, due to the crossover nature of these transitions and a finite width of both transitions, the confinement and chiral restoration never set exactly at the mentioned intermediate region of temperatures. Nevertheless, this intermediate phase is characterized by a nonzero  $\sigma$  condensate (a chirally broken regime) and a nonzero expectation value of the Polyakov loop  $L$  (a deconfinement regime). This splitting effect produced by the finite size of the system becomes stronger for a denser system.

Thus, the softening, shifting and splitting of the chiral and deconfining transitions are finite-volume effects.

#### 2. Quantifying the splitting of transition temperatures

How strong is the splitting in chiral and deconfining temperatures? To this end, we found the inflection points in the chiral order parameter,  $\sigma$ , and in the deconfining order parameter,  $L$  (determined, as usual, along a diagonal line crossing the origin of the parameter space,  $T = \mu = 0$ ). We plot the crossover temperatures in Fig. 5(a) at a fixed radius of the system  $R$  as a function of the chemical potential  $\mu$  and vice versa, at a set of fixed chemical potentials as the function of the radius of the cylinder  $R$ .

Figure 5(a) demonstrates that the splitting takes its maximal value at vanishing chemical potential,  $\mu = 0$ . As the chemical potential increases, the splitting decreases. Thus, the finite-volume effect of the splitting gets reduced in the finite-density system. Moreover, we see the already noticed property that the decrease in the radius of the cylinder increases the splitting.

The finite-volume splitting effect is rather noticeable at  $R = 1$  fm, where the difference in temperature achieves a rather modest 5 – 6% of the pseudo-critical temperature. However, in this case, the radius of the cylinder is about the size of the hadron, so that at this size, strictly speaking, the system is not in a bulk state, at least with respect to the transverse directions. In other words, there is space only for two or three hadrons to fit into the transverse plane of the area  $A_{\perp} \simeq 3.14 \text{ fm}^2$ , which does not allow us to consider this system as a thermodynamically large ensemble, at least, in the transverse directions.

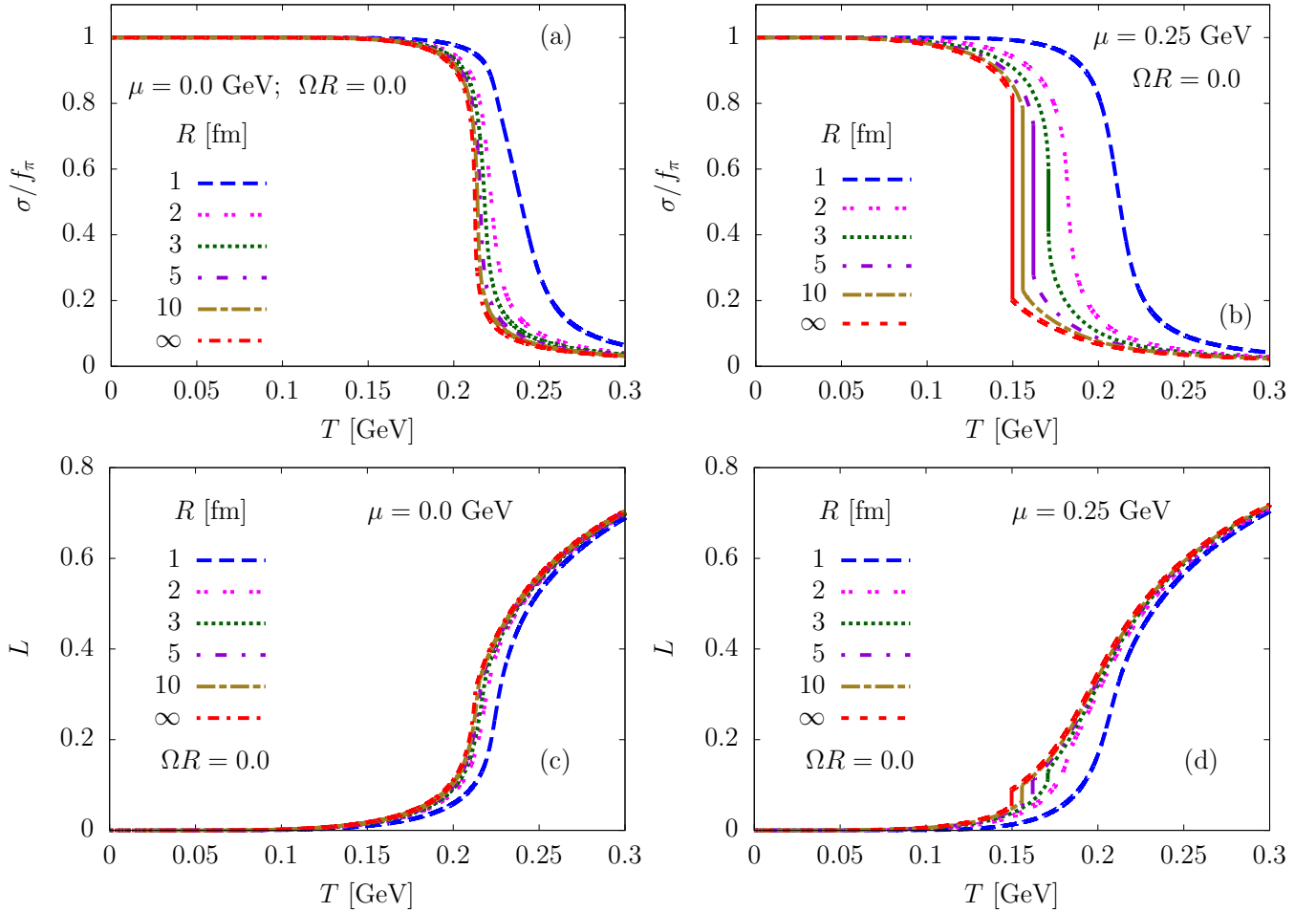


FIG. 4. The dependence on temperature of (top) the normalized chiral order parameter  $\sigma/f_\pi$  and (bottom) the confinement order parameters  $L$  and  $L^*$  for a static ( $\Omega R = 0$ ) cylindrical system of various radii for (left) vanishing,  $\mu = 0$  and (right) a non-zero,  $\mu = 0.25$  GeV, chemical potentials.

However, already at  $R = 3$  fm, the splitting of the chiral and deconfining transitions is barely noticeable. The transverse area becomes rather large,  $A_\perp \simeq 28 \text{ fm}^2$ , which allows us to consider this system as a bulk medium that gets closer to the thermodynamic limit,  $R \rightarrow \infty$ . And, in agreement with almost no splitting found at  $R = 3$  fm, there is no splitting between the transitions in the thermodynamic limit, as we have found in the previous section.

Figure 5(b) allows us to quantify the magnitude of the splitting as a function of the radius. For presentation reasons, it is convenient to plot the split in the pseudo-critical temperatures of chiral,  $T_c^{(\sigma)}$ , and deconfining,  $T_c^{(L)}$ , transitions:

$$\Delta T_c = T_c^{(\sigma)} - T_c^{(L)} > 0, \quad (57)$$

as a function of the inverse radius,  $1/R$ . This Figure nicely illustrates two properties of the non-rotating system: both the increase in the radius of the cylinder and the increase of the baryon density of the medium inside the cylinder diminish the split. For the discussed

$R = 3$  fm cylinder, which can loosely be considered a bulk system, the finite-size splitting amounts to a tiny  $\Delta T_{pc} \sim 1$  MeV at zero-density plasma ( $\mu = 0$ ). Notice that to maintain consistency in our notation, we denote the pseudo-critical temperatures  $T_{pc}$  also by  $T_c$ .

After determining the effect of the finite volume on the splitting of the transition temperatures, we can look at the impact of rotation on the bulk properties of the system, such as the phase transition diagram. Here, the word “bulk” implies that we neglect the surface effect of the boundary related to the existence of the mass gap of the system. In a system with a mass gap  $M$ , the boundary affects the properties of the system given by the distance of one correlation length  $\lambda = 1/M$  from the boundary. The phenomena found in this section so far can be considered as the manifestation of this effect.

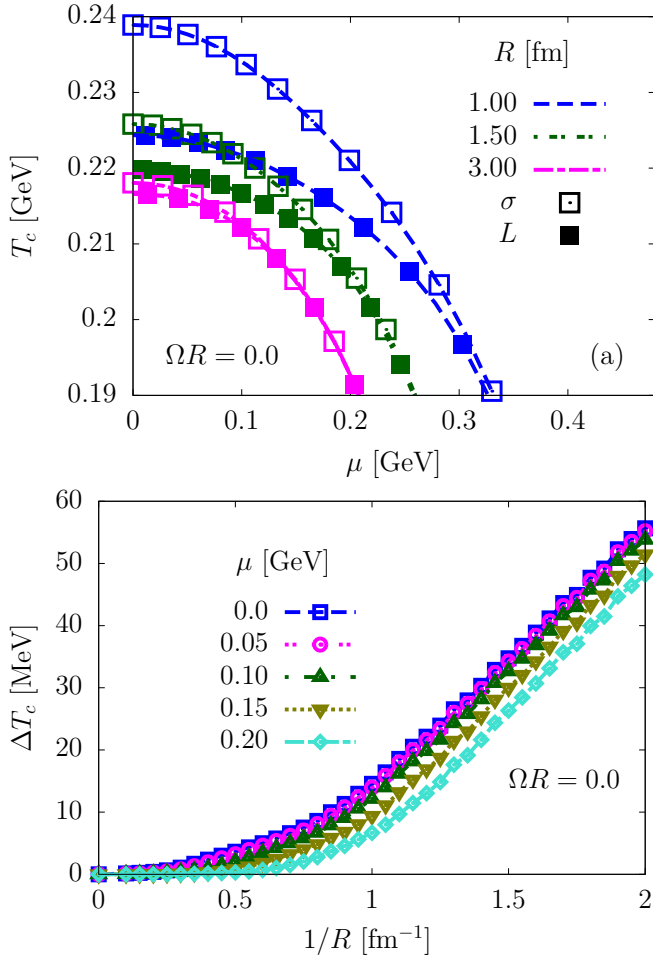


FIG. 5. (a) The crossover temperatures as a function of the chemical potential  $\mu$  for the chiral transition and the deconfinement transition determined from the inflection points of the  $\sigma$  condensate and  $L$  (or  $L^*$ ). Several values of the radius of the cylinder are shown. (b) The split in the transition temperatures (57) for chiral and confinement-deconfinement crossovers at different fixed chemical potentials as a function of the (inverse) radius. All plots are shown for zero angular velocity,  $\Omega R = 0$ .

### B. Effect of rotation on temperature splitting

We now consider the pseudocritical transition temperatures  $T_{pc}^{(\sigma)}$  and  $T_{pc}^{(L)}$  at finite volume and with rotation for the case when  $\mu = 0$ , when the split (57) between these two temperatures is maximal, as shown in Fig. 6. Panel (a) of Fig. 6 shows the dependence of both  $T_c(L)$  (upper, dashed lines with empty symbols) and  $T_c(\sigma)$  (the lower, solid lines with the filled symbols) on the radius of the cylindrical boundary, for various values of the rotation parameter, taken such that  $\Omega R = 0$  (the blue lines and the rhombi), 0.9 (the orange lines and the triangles), 0.98 (the green lines and the circles) and 1 (purple lines and squares) is kept fixed. When  $\Omega R < 1$ , it can be seen that the gap  $T_{pc}^{(L)} - T_{pc}^{(\sigma)}$  reduces as  $R$  is increased,

becoming negligible when  $R \gtrsim 2$  fm. In the case when  $\Omega R = 1$ , the gap never fully disappears.

In panel (b) of Figure 6, we show the difference  $\Delta T_{pc}$  of the transition temperatures (57) as a function of the inverse radius of the cylinder,  $1/R$ , at various rotation frequencies  $\Omega R$ . The results are shown for vanishing chemical potential,  $\mu = 0$ , where the splitting takes its maximum value. One can clearly see that the rotation does not increase the splitting. On the contrary, the difference in temperatures between the chiral and deconfining transitions, generated by the finite-volume effects, becomes even smaller as the rotation frequency increases.

Thus, rotation inhibits the splitting of temperatures rather than producing it.

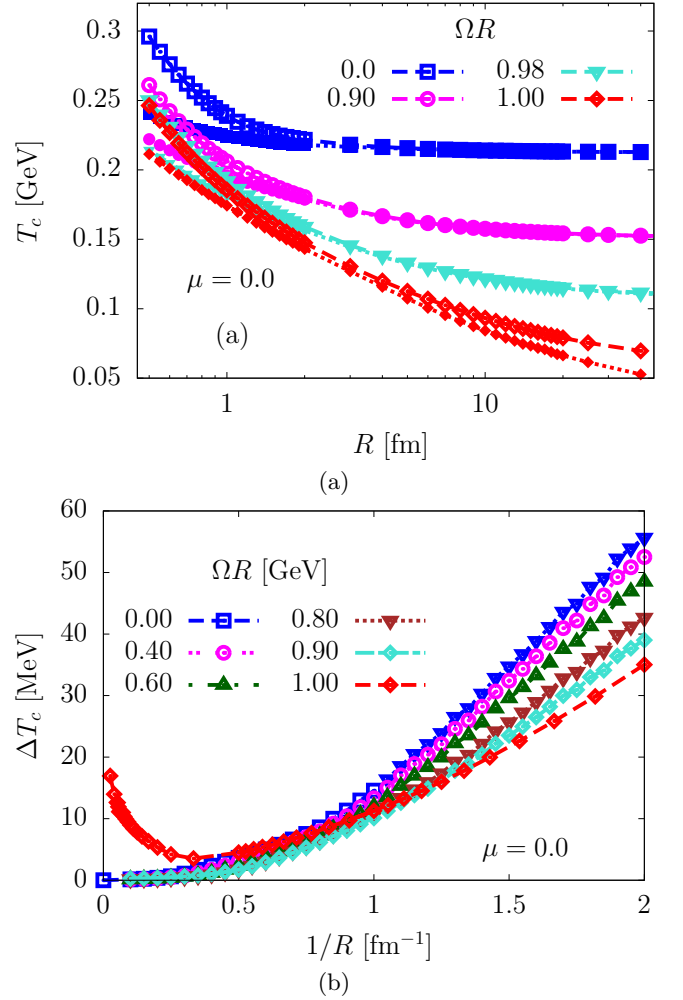


FIG. 6. Effect of rotation on the separation of chiral and deconfinement crossovers: (a) the pseudocritical temperatures as a function of  $R$  and (b) their difference  $\Delta T_c$  (57) as a function of  $1/R$  at different values of  $\Omega R$ . The results are shown for vanishing chemical potential  $\mu = 0$ , which gives the maximum temperature difference  $\Delta T_c$ . In panel (a), the empty (filled) symbols correspond to chiral (deconfinement) transitions.

Let us relate the results shown in Fig. 6 to the physical conditions corresponding to the realistic conditions of the

vortical plasmas produced in the relativistic heavy-ion collisions. In the RHIC experiment, the vorticity of the quark-gluon plasma corresponds to the angular frequency of  $\Omega \simeq 6.6$  MeV [2], which translates to  $\Omega R \simeq 0.165$  for a system of a rather large size  $R = 5$  fm. Thus, the rotation velocity at the boundary of the system is much smaller than the ultrarelativistic limit  $\Omega R = 1$ . To put this number in a different perspective, the rotational Lorentz factor at the edge of the system for RHIC-type collisions amounts to  $1/\sqrt{1 - (\Omega R)^2} \approx 1.01$ , providing us with a minuscule one-percent increase. In other words, the effect of the presence of the boundary of a rotating system on the thermodynamic properties of this system is much larger than the effect of the rotation itself.

Consider also an academic limit of the ultrarelativistic vorticities, for which the parameter  $\Omega R$  reaches  $\Omega R = 1$  value. Since at such rotation, the matter effects may potentially be also important, in Fig. 7, we plot the splitting as the function of  $\Omega R$  for various values of the chemical potential  $\mu$  at different sizes  $R$  of the system. The results confirm that, similarly to the finite-volume effects, the increasing chemical potential inhibits the split in the transition temperatures. Moreover, for all chemical potential, the increase of the rotation frequency up to  $\Omega R \simeq 0.9$  inhibits the temperature difference. However, at event faster rotations, as  $\Omega R \rightarrow 1$ , the splitting in the transition temperature starts to increase, reaching a larger value at  $\Omega R = 1$ . Still, even at  $\mu = 0$ , the rotation-induced splitting in the academic ultrarelativistic regime reaches a rather moderate value,  $\Delta T_c \simeq 11$  MeV.

According to Fig. 7, the split in the transition temperature appears to grow when  $\Omega R$  approaches the maximal value limited by the causality,  $\Omega R = 1$ . As can be seen in panel (a) of Fig. 6, the gap  $\Delta T_c(\Omega R = 1)$  initially decreases with increasing  $R$ , while when  $R$  increases beyond 3 fm, it increases. Since the split appears due to a lower pseudocritical temperature for the Polyakov loop  $L$  than for  $\sigma$ , we can expect that the gap  $\Delta T_c$  widens with increasing  $R$  and then again shrinks, as for both  $L$  and  $\sigma$ ,  $T_c \rightarrow 0$  when  $R \rightarrow \infty$ . We note, however, that probing this large- $R$  regime is computationally expensive, and we therefore leave it for the more detailed analysis in our forthcoming publication [42].

Finally, we would like to comment on the nature of the crossover transition in the regime where the chiral and deconfinement transition temperatures do not coincide. Panel (a) of Fig. 8 shows the temperature dependence of both the sigma meson  $\sigma$  and the Polyakov loop  $L$ , in the case when  $R = 3$  fm and  $\mu = 0$ , for  $\Omega R = 0, 0.8$  and 1. These values of  $\Omega R$  were chosen to correspond to the maximum value of  $\Delta T_{pc}$ , its minimum value, and again the peak reached at the causality limit, respectively. Looking at the plot, we can see that the chiral and deconfinement transitions are very much overlapped and no clear distinction between their respective pseudocritical transition temperatures can be seen. Panel (b) of the same figure shows the scaled slopes  $\mathcal{N}\partial\sigma/\partial T$  and  $\partial L/\partial T$ , in the above cases. Here the normalization  $\mathcal{N}$  is

such that the peak of  $\partial\sigma/\partial T$  lies at the same value as that of  $\partial L/\partial T$ . While the peaks of these slopes, used by us to identify the corresponding pseudocritical temperature, do not coincide, the bell-shaped area developing around these peaks is overlapped. We can thus conclude that a discussion of a unique value for the pseudocritical temperature, and hence the identification of a split between deconfinement and chiral symmetry restoration, is at best ambiguous in the case of rotating systems.

## V. CONCLUSIONS

In our paper, we discussed how the rigid rotation of quark-gluon plasma, modeled by the Polyakov-loop enhanced linear sigma model with quarks, affects the critical temperatures of deconfinement and chiral transitions. We highlighted the importance of the causality condition, which requires that any point in the system rotates slower than the speed of light. Since the rotation is rigid, the causality condition limits the size of the system in the transverse directions,  $R < 1/\Omega$ , where  $\Omega > 0$  is the angular frequency.

We have found that the confinement and chiral transitions split in the system. However, this splitting effect originates not due to the rotation of the system but rather due to its finite volume. In a very small non-rotating system with a radius of one fermi, the splitting can reach a modest  $\Delta T_c \sim 10$  MeV, which is comparable with the width of the crossover transition [54–56]. For systems of the size of about 3-5 fm, the splitting becomes very negligible,  $\Delta T \sim 1$  MeV.

Contrary to expectations, the rotation appears to inhibit this finite-volume splitting: as the angular velocity increases, the chiral and deconfining temperatures approach each other. The splitting is also inhibited by a finite chemical potential: as the density of the plasma increases, the splitting between the chiral and confining transitions becomes smaller.

We have also considered an ultra-relativistic regime where the boundary of the system rotates very close to the speed of light. In this, the temperature splitting becomes visible again, but it still remains in the modest 10 MeV range.

One should stress that we used the uniform approximation, in which both the chiral condensate and the expectation value of the Polyakov loop are treated as coordinate-independent quantities. This approach, which can be justified for a central region of plasma that rotates with a slow rotational velocity,  $\Omega R \ll 1$ , can not be applied for rapidly rotating, in the sense of the boundary velocity, systems with  $\Omega R \sim 1$ . For such plasmas, the inhomogeneities must be taken into account. Still, we believe that the results of this paper, obtained in the uniform approximation, are applicable to realistic plasmas that rotate relatively slowly.

We conclude that rotation is unlikely to induce the splitting between chiral and confining transitions in re-

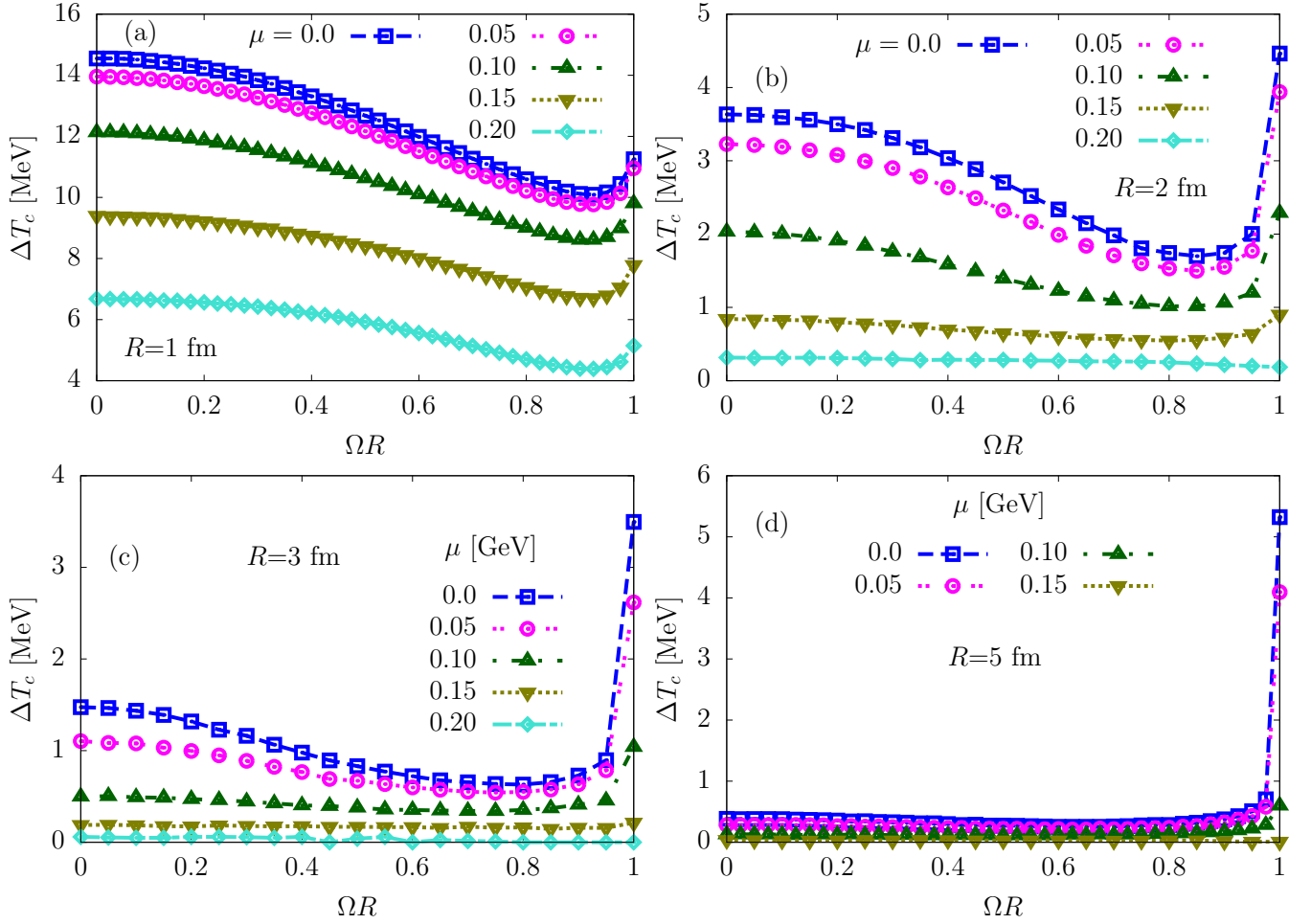


FIG. 7. Difference in the crossover temperatures  $\Delta T_c$  for chiral and confinement-deconfinement transitions at different values of the chemical potential  $\mu$  as a function of angular velocity, given in units of  $\Omega R$ . Each plot corresponds to a fixed radius of the cylinder,  $R = (1, 2, 3, 5)$  fm.

alistic vortical plasmas created in relativistic heavy-ion collisions.

## ACKNOWLEDGMENTS

This work is supported by the European Union - NextGenerationEU through grant No. 760079/23.05.2023, funded by the Romanian ministry of research, innovation and digitalization through Romania's National Recovery and Resilience Plan, call no. PNRR-III-C9-2022-I8.

- 
- [1] B. I. Abelev et al. (STAR), “Global polarization measurement in Au+Au collisions,” *Phys. Rev. C* **76**, 024915 (2007), [Erratum: *Phys.Rev.C* 95, 039906 (2017)], [arXiv:0705.1691 \[nucl-ex\]](#).
- [2] L. Adamczyk et al. (STAR), “Global  $\Lambda$  hyperon polarization in nuclear collisions: evidence for the most vortical fluid,” *Nature* **548**, 62–65 (2017), [arXiv:1701.06657 \[nucl-ex\]](#).
- [3] Xu-Guang Huang, Jinfeng Liao, Qun Wang, and Xiao-Liang Xia, “Vorticity and Spin Polarization in Heavy Ion Collisions: Transport Models,” *Lect. Notes Phys.* **987**, 281–308 (2021), [arXiv:2010.08937 \[nucl-th\]](#).
- [4] Francesco Becattini, Jinfeng Liao, and Michael Lisa, “Strongly Interacting Matter Under Rotation: An Introduction,” *Lect. Notes Phys.* **987**, 1–14 (2021), [arXiv:2102.00933 \[nucl-th\]](#).
- [5] Arata Yamamoto and Yuji Hirono, “Lattice QCD in rotating frames,” *Phys. Rev. Lett.* **111**, 081601 (2013), [arXiv:1303.6292 \[hep-lat\]](#).

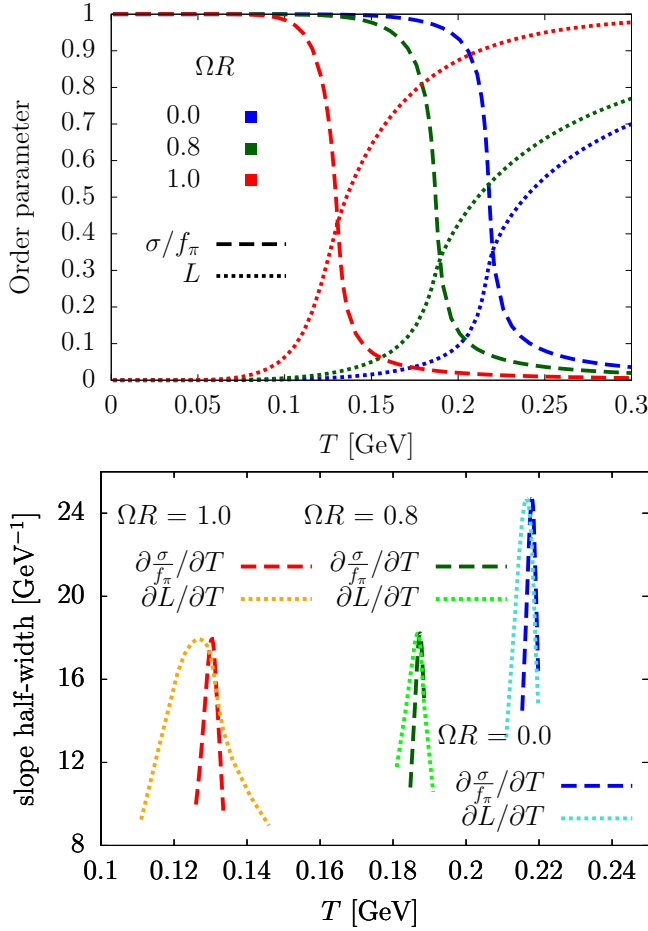


FIG. 8. Variation of (a) the  $\sigma$  and  $L$  order parameters; and (b) the slopes  $\partial(\sigma/f_\pi)/\partial T$  and  $\partial L/\partial T$ , with respect to the temperature  $T$ , for a system of size  $R = 3$  fm, at various values of  $\Omega R$  at  $\mu = 0$ .

- [6] V. V. Braguta, A. Yu. Kotov, D. D. Kuznedelev, and A. A. Roenko, “Study of the Confinement/Deconfinement Phase Transition in Rotating Lattice SU(3) Gluodynamics,” *Pisma Zh. Eksp. Teor. Fiz.* **112**, 9–16 (2020).
- [7] V. V. Braguta, A. Yu. Kotov, D. D. Kuznedelev, and A. A. Roenko, “Influence of relativistic rotation on the confinement-deconfinement transition in gluodynamics,” *Phys. Rev. D* **103**, 094515 (2021), arXiv:2102.05084 [hep-lat].
- [8] V. V. Braguta, Andrey Kotov, Artem Roenko, and Dmitry Sychev, “Thermal phase transitions in rotating QCD with dynamical quarks,” *PoS LATTICE2022*, 190 (2023), arXiv:2212.03224 [hep-lat].
- [9] V. V. Braguta, I. E. Kudrov, A. A. Roenko, D. A. Sychev, and M. N. Chernodub, “Lattice Study of the Equation of State of a Rotating Gluon Plasma,” *JETP Lett.* **117**, 639–644 (2023).
- [10] Victor V. Braguta, Maxim N. Chernodub, Artem A. Roenko, and Dmitrii A. Sychev, “Negative moment of inertia and rotational instability of gluon plasma,” *Phys. Lett. B* **852**, 138604 (2024), arXiv:2303.03147 [hep-lat].
- [11] Ji-Chong Yang and Xu-Guang Huang, “QCD on Rotating Lattice with Staggered Fermions,” (2023), arXiv:2307.05755 [hep-lat].
- [12] Victor V. Braguta, Maxim N. Chernodub, and Artem A. Roenko, “New mixed inhomogeneous phase in vortical gluon plasma: First-principle results from rotating SU(3) lattice gauge theory,” *Phys. Lett. B* **855**, 138783 (2024), arXiv:2312.13994 [hep-lat].
- [13] Victor V. Braguta, Maxim N. Chernodub, Ilya E. Kudrov, Artem A. Roenko, and Dmitrii A. Sychev, “Negative Barnett effect, negative moment of inertia of (quark-)gluon plasma and thermal evaporation of chromomagnetic condensate,” (2023), arXiv:2310.16036 [hep-ph].
- [14] M. Gell-Mann and M. Lévy, “The axial vector current in beta decay,” *Il Nuovo Cimento* **16**, 705–726 (1960).
- [15] Adrian Dumitru and Robert D. Pisarski, “Event-by-event fluctuations from decay of a Polyakov loop condensate,” *Phys. Lett. B* **504**, 282–290 (2001), arXiv:hep-ph/0010083.
- [16] O. Scavenius, A. Dumitru, and A. D. Jackson, “Explosive decomposition in ultrarelativistic heavy ion collision,” *Phys. Rev. Lett.* **87**, 182302 (2001), arXiv:hep-ph/0103219.
- [17] O. Scavenius, A. Dumitru, and J. T. Lenaghan, “The  $K/\pi$  ratio from condensed Polyakov loops,” *Phys. Rev. C* **66**, 034903 (2002), arXiv:hep-ph/0201079.
- [18] E. Megias, E. Ruiz Arriola, and L. L. Salcedo, “Polyakov loop in chiral quark models at finite temperature,” *Phys. Rev. D* **74**, 065005 (2006), arXiv:hep-ph/0412308.
- [19] Bernd-Jochen Schaefer, Jan M. Pawłowski, and Jochen Wambach, “The Phase Structure of the Polyakov–Quark-Meson Model,” *Phys. Rev. D* **76**, 074023 (2007), arXiv:0704.3234 [hep-ph].
- [20] Hao-Lei Chen, Kenji Fukushima, Xu-Guang Huang, and Kazuya Mameda, “Analogy between rotation and density for Dirac fermions in a magnetic field,” *Phys. Rev. D* **93**, 104052 (2016), arXiv:1512.08974 [hep-ph].
- [21] Yin Jiang and Jinfeng Liao, “Pairing Phase Transitions of Matter under Rotation,” *Phys. Rev. Lett.* **117**, 192302 (2016), arXiv:1606.03808 [hep-ph].
- [22] M. N. Chernodub and Shinya Gongyo, “Effects of rotation and boundaries on chiral symmetry breaking of relativistic fermions,” *Phys. Rev. D* **95**, 096006 (2017), arXiv:1702.08266 [hep-th].
- [23] Xinyang Wang, Minghua Wei, Zhibin Li, and Mei Huang, “Quark matter under rotation in the NJL model with vector interaction,” *Phys. Rev. D* **99**, 016018 (2019), arXiv:1808.01931 [hep-ph].
- [24] Xun Chen, Lin Zhang, Danning Li, Defu Hou, and Mei Huang, “Gluodynamics and deconfinement phase transition under rotation from holography,” *JHEP* **07**, 132 (2021), arXiv:2010.14478 [hep-ph].
- [25] S. M. A. Tabatabaee Mehr and F. Taghinavaz, “Chiral phase transition of a dense, magnetized and rotating quark matter,” *Annals Phys.* **454**, 169357 (2023), arXiv:2201.05398 [hep-ph].
- [26] Yan-Qing Zhao, Song He, Defu Hou, Li Li, and Zhibin Li, “Phase diagram of holographic thermal dense QCD matter with rotation,” *JHEP* **04**, 115 (2023), arXiv:2212.14662 [hep-ph].
- [27] Hao-Lei Chen, Zhi-Bin Zhu, and Xu-Guang Huang, “Quark-meson model under rotation: A functional renormalization group study,” *Phys. Rev. D* **108**, 054006 (2023), arXiv:2306.08362 [hep-ph].

- [28] Fei Sun, Shuang Li, Rui Wen, Anping Huang, and Wei Xie, “The rotation effect on the thermodynamics of the QCD matter,” (2023), [arXiv:2310.18942 \[hep-ph\]](#).
- [29] S. J. Barnett, “Magnetization by Rotation,” *Phys. Rev. B* **6**, 239 (1915).
- [30] Fei Sun, Jingdong Shao, Rui Wen, Kun Xu, and Mei Huang, “Chiral phase transition and spin alignment of vector mesons in the polarized-Polyakov-loop Nambu–Jona-Lasinio model under rotation,” *Phys. Rev. D* **109**, 116017 (2024), [arXiv:2402.16595 \[hep-ph\]](#).
- [31] Kenji Fukushima, “Chiral effective model with the Polyakov loop,” *Phys. Lett. B* **591**, 277–284 (2004), [arXiv:hep-ph/0310121](#).
- [32] Simon Roessner, Claudia Ratti, and W. Weise, “Polyakov loop, diquarks and the two-flavour phase diagram,” *Phys. Rev. D* **75**, 034007 (2007), [arXiv:hep-ph/0609281](#).
- [33] R. L. S. Farias, V. S. Timoteo, S. S. Avancini, M. B. Pinto, and G. Krein, “Thermo-magnetic effects in quark matter: Nambu–Jona-Lasinio model constrained by lattice QCD,” *Eur. Phys. J. A* **53**, 101 (2017), [arXiv:1603.03847 \[hep-ph\]](#).
- [34] Fei Sun, Kun Xu, and Mei Huang, “Splitting of chiral and deconfinement phase transitions induced by rotation,” *Phys. Rev. D* **108**, 096007 (2023), [arXiv:2307.14402 \[hep-ph\]](#).
- [35] Paul C. W. Davies, Tevian Dray, and Corinne A. Manogue, “The Rotating quantum vacuum,” *Phys. Rev. D* **53**, 4382–4387 (1996), [arXiv:gr-qc/9601034](#).
- [36] O. Scavenius, A. Mocsy, I. N. Mishustin, and D. H. Rischke, “Chiral phase transition within effective models with constituent quarks,” *Phys. Rev. C* **64**, 045202 (2001), [arXiv:nucl-th/0007030](#).
- [37] Robert D. Pisarski and Frank Wilczek, “Remarks on the Chiral Phase Transition in Chromodynamics,” *Phys. Rev. D* **29**, 338–341 (1984).
- [38] O. Scavenius, A. Dumitru, E. S. Fraga, J. T. Lenaghan, and A. D. Jackson, “First order chiral phase transition in high-energy collisions: Can nucleation prevent spinodal decomposition?” *Phys. Rev. D* **63**, 116003 (2001), [arXiv:hep-ph/0009171](#).
- [39] V. Skokov, B. Stokic, B. Friman, and K. Redlich, “Meson fluctuations and thermodynamics of the Polyakov loop extended quark-meson model,” *Phys. Rev. C* **82**, 015206 (2010), [arXiv:1004.2665 \[hep-ph\]](#).
- [40] Simon Roessner, T. Hell, C. Ratti, and W. Weise, “The chiral and deconfinement crossover transitions: PNJL model beyond mean field,” *Nucl. Phys. A* **814**, 118–143 (2008), [arXiv:0712.3152 \[hep-ph\]](#).
- [41] Joseph I. Kapusta and Charles Gale, [Finite-Temperature Field Theory: Principles and Applications](#), 2nd ed., Cambridge Monographs on Mathematical Physics (Cambridge University Press, 2006).
- [42] Pracheta Singha, Victor E. Ambrus, and M. N. Chernodub, “Inhibition of splitting of the chiral and deconfinement transition due to rotation in QCD: the phase diagram of linear sigma model coupled to Polyakov loop,” in preparation (2024).
- [43] Claudia Ratti, Simon Roessner, and Wolfram Weise, “Quark number susceptibilities: Lattice QCD versus PNJL model,” *Phys. Lett. B* **649**, 57–60 (2007), [arXiv:hep-ph/0701091](#).
- [44] Juan M. Torres-Rincon and Joerg Aichelin, “Equation of state of a quark-meson mixture in the improved Polyakov–Nambu–Jona-Lasinio model at finite chemical potential,” *Phys. Rev. C* **96**, 045205 (2017), [arXiv:1704.07858 \[nucl-th\]](#).
- [45] Kouji Kashiwa, Hiroaki Kouno, Masayuki Matsuzaki, and Masanobu Yahiro, “Critical endpoint in the Polyakov-loop extended NJL model,” *Phys. Lett. B* **662**, 26–32 (2008), [arXiv:0710.2180 \[hep-ph\]](#).
- [46] Victor E. Ambrus and Elizabeth Winstanley, “Rotating quantum states,” *Phys. Lett. B* **734**, 296–301 (2014), [arXiv:1401.6388 \[hep-th\]](#).
- [47] M. N. Chernodub and Shinya Gongyo, “Interacting fermions in rotation: chiral symmetry restoration, moment of inertia and thermodynamics,” *JHEP* **01**, 136 (2017), [arXiv:1611.02598 \[hep-th\]](#).
- [48] L D Landau and E M Lifshitz, *Mechanics*, 3rd ed. (Butterworth-Heinemann, Oxford, England, 1982).
- [49] L. D. Landau and E. M. Lifshitz, *Statistical Physics*, 3rd ed. (Butterworth-Heinemann, Oxford, England, 1996).
- [50] Victor E. Ambrus and Elizabeth Winstanley, “Rotating fermions inside a cylindrical boundary,” *Phys. Rev. D* **93**, 104014 (2016), [arXiv:1512.05239 \[hep-th\]](#).
- [51] M. Hortacsu, K. D. Rothe, and B. Schroer, “Zero Energy Eigenstates for the Dirac Boundary Problem,” *Nucl. Phys. B* **171**, 530–542 (1980).
- [52] M. N. Chernodub, “Inhomogeneous confining-deconfining phases in rotating plasmas,” *Phys. Rev. D* **103**, 054027 (2021), [arXiv:2012.04924 \[hep-ph\]](#).
- [53] M. N. Chernodub, V. A. Goy, and A. V. Molochkov, “Inhomogeneity of a rotating gluon plasma and the Tolman-Ehrenfest law in imaginary time: Lattice results for fast imaginary rotation,” *Phys. Rev. D* **107**, 114502 (2023), [arXiv:2209.15534 \[hep-lat\]](#).
- [54] Y. Aoki, Z. Fodor, S. D. Katz, and K. K. Szabo, “The QCD transition temperature: Results with physical masses in the continuum limit,” *Phys. Lett. B* **643**, 46–54 (2006), [arXiv:hep-lat/0609068](#).
- [55] Szabolcs Borsanyi, Zoltan Fodor, Christian Hoelbling, Sandor D Katz, Stefan Krieg, Claudia Ratti, and Kalman K. Szabo (Wuppertal-Budapest), “Is there still any  $T_c$  mystery in lattice QCD? Results with physical masses in the continuum limit III,” *JHEP* **09**, 073 (2010), [arXiv:1005.3508 \[hep-lat\]](#).
- [56] A. Bazavov et al., “The chiral and deconfinement aspects of the QCD transition,” *Phys. Rev. D* **85**, 054503 (2012), [arXiv:1111.1710 \[hep-lat\]](#).